Concurrent static and dynamic light scattering from macromolecular solutions. 1. Model systems in the low q regime

Thomas A. P. Seery, Jeffrey A. Shorter* and Eric J. Amis†
Department of Chemistry, University of Southern California, Los Angeles, CA 90089-0482, USA
(Received 16 February 1988; revised 15 September 1988; accepted 25 September 1988)

Concurrent acquisition of static and dynamic light scattering data has been performed on model systems of dilute narrow molecular weight distribution polystyrenes in toluene and also on dilute suspensions of monodisperse polystyrene lattices in water. The data were analysed to extract a self consistent set of thermodynamic (molecular weight, radius of gyration, virial coefficient) and hydrodynamic (diffusion coefficient) results. It is demonstrated that the intensity autocorrelation function can be analysed to determine the absolute magnitude of the temporal–spatial scattering surface and can therefore provide the results which would normally be obtained from a separate static light scattering experiment. Preliminary results in the intermediate q regime suggest that with a concurrent analysis scheme of the type demonstrated here it will be possible to analyse in further detail the transition of the scattering function from q^2 to q^3 dependence.

(Keywords: dynamic light scattering; static light scattering; intermediate q regime)

INTRODUCTION

Over the past fifteen years, advances in the theory and technology of light scattering have made it a powerful tool for the investigation of macromolecular systems. Some of the recent applications of static light scattering, s.l.s., and dynamic light scattering, d.l.s., have included studies of semidilute solutions[1–5], the intermediate q regime[6], polydispersity analysis[7], and mixed polymer systems with refractive index matching[8–10]. Each of these applications have helped to characterize various aspects of macromolecular dynamics, which in turn tested and sharpened our understanding of polymer physics[11–14]. At the same time, d.l.s. often seems to be a technique which does not quite live up to its potential. In principle it is a very powerful, nonperturbative tool which allows one to probe the dynamics of macromolecules. Nevertheless, new applications for the technique have often been hampered because of ambiguities in the interpretations of the measurements.

The source of light scattered from polymer solutions is thermodynamically driven concentration fluctuations. These fluctuations are dissipated on temporal and spatial scales dependent on the interaction of thermodynamic and hydrodynamic forces with molecular properties of size, shape, stiffness, etc. We can probe these interactions using s.l.s. and d.l.s. The difference between s.l.s. and d.l.s. is not in the physics of scattered light but in how the scattered light is collected, analysed, and processed with the instrumentation. Because it is the same light which is scattered by the molecules, independent of whether we detect and analyse it as s.l.s. or d.l.s., our ultimate goal is to combine the information obtained by the two analyses to yield a self-consistent interpretation of complex scattering processes.

Historically, s.l.s. was developed and refined many years before the advances of lasers and electronics made d.l.s. possible. In an appropriate instrument, the classic s.l.s. technique measures the time integrated, total scattering intensity as a function of scattering angle and polymer concentration. This yields equilibrium properties which include the weight average molecular weight M_w, osmotic second virial coefficient A_2, and z-average radius of gyration $\langle R_G \rangle_z$.

In a d.l.s. experiment the emphasis is on determining the decay constants for the intensity–intensity autocorrelation function of the scattered light. Information about the total scattering intensity is discarded during the normalization. Typically d.l.s. is practiced in isolation from s.l.s. with instrumentation optimized for measurement of the time autocorrelation function. The decay constant is extracted from the dynamic correlation function and is interpreted to yield mutual diffusion coefficients[11], cooperative ('pseudo gel') diffusion coefficients[1–4], and internal relaxation modes[6]. For monodisperse, noninteracting scattering centres, excellent values of the mutual diffusion coefficient are directly obtained and, by extrapolation to zero concentration, the self diffusion coefficient can be determined. Unfortunately, there are a significant number of systems, such as solutions at higher concentrations, mixtures of polymers and rod-like molecules, where these simple procedures (either for static or dynamic scattering) do not work well and the interpretations become very difficult[12].

As a first step in developing a concurrent analysis scheme, we have simultaneously collected data in both static and dynamic modes for simple, well controlled, model systems: dilute water suspensions of monodisperse lattices, and dilute toluene solutions of narrow distribu-

* Present address: Department of Chemistry, Massachusetts Institute of Technology, Cambridge, MA, USA
† To whom correspondence should be addressed

0032-3861/89/071197-07$03.00

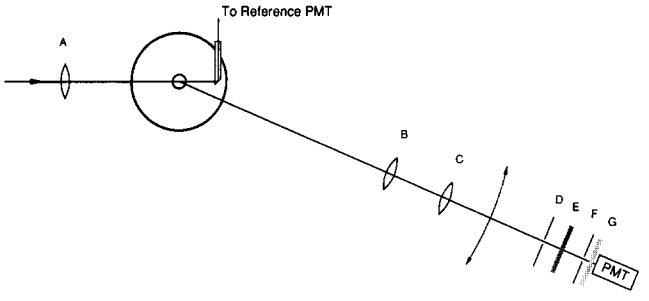

Figure 1 Schematic diagram of goniometer optical path. (A)100 mm lens focuses the laser through the index matching vat into a scattering cell; (B) 200 mm lens and (C) 100 mm lens images scattering centre onto (D) 200 μm vertical slit; (E) laser line interference filter and (F) variable (50 μm–3 mm) aperture select a fraction of imaged light which is diffused by (G) a frosted plate onto the photocathode of the photomultiplier tube. Receiving optics (B–G) rotate to accept scattering angles from 10 to 160°

tion polystyrenes. We have produced identical Zimm plots from the total intensity data and from the autocorrelation data. Using the same method we have also placed the temporal and spatial scattering surface on an absolute intensity scale. For the simple cases we have obtained self-consistent thermodynamic and hydrodynamic parameters. At the same time, we anticipate that these methods may address problems such as occur in the interpretation of the intermediate q regime.

EXPERIMENTAL

Instrumentation

Goniometer. All of the light scattering measurements were made using an Ar ion laser (Spectra Physics 2020-3) operating at 514.5 nm with 200 to 500 mW. A commercial light scattering goniometer (Brookhaven Instruments BI-200SM) with stepping motor control was used to collect data at scattering angles from 30 to 150° at increments of 5°. The original integrated optical components of the commercial goniometer were used to direct the incident beam through the sample and to collect the scattered light at precise angles. *Figure 1* illustrates the optical path. A few modifications in the alignment procedures and the addition of a diffusing filter before the photocathode of the PMT were necessary. The PMT (Thorn EMI 9863B), tested and selected for low dark count and low afterpulsing, was used in photon counting mode in a shielded, room temperture housing with integrated amplifier-discriminator (Thorn EMI AD100). From inside the temperature controlled (Haake A81) refractive index matching bath of filtered toluene, the transmitted intensity was collected by a periscope of neutral density material and channelled with a fibre optic to a second matched PMT. There are some special considerations which must be taken into account in the optical system for a combined static and dynamic-scattering instrument. These are discussed below.

The absolute magnitude of the scattered intensity is directly proportional to the illuminated volume observed by the detector. This volume must be reproducible and well defined. Our scattering geometry consists of a cylindrical vat with a flat entrance window and cylindrical sample tubes which are concentrically located about the centre of rotation of the detection optics. For a cylindrically symmetric laser beam in this geometry, the detection optics define a scattering volume which is inversely proportional to sine of the scattering angle. We correct for this by multiplying the scattering intensity by $\sin\theta$. Reflections at the flat entrance window are minimized by filling the vat with toluene, an index matching fluid. This is also the solvent for the experiment and because its index of refraction is so close to the index of glass, spurious reflections from the vat and the cell are minimal. For the same reason we can thus neglect refraction corrections to the observed solid angle which might be necessary with a different solvent.

The incoming laser beam is aligned through two 2 mm apertures and is focused with a 100 mm focal length lens to a diameter of approximately 50 μm in the centre of the sample cell[14]. The detection optics consist of two lenses, a slit, and a variable aperture. The first lens, with a 200 mm focal length, collimates the scattered light. This is then refocused by the second lens (100 mm focal length) onto a 200 μm vertical slit. The image of the scattering volume is thus expanded by the ratio of focal lengths so that 100 μm of the beam waist illuminating the sample is imaged onto the 200 μm slit.

The linear dimension of a scattering coherence area may be estimated as $k\lambda R/L$ with λ being the wavelength, R the distance from the image source to the detector, L the linear dimension of the source, and k a constant which is argued to lie between 1 and 4 (ref. 14). Our detector is located 75 mm from the slit, and the image of the scattering volume matches the slit dimension. With k between 1 and 4 the linear dimension of the coherence area on the detector could be between 200 and 800 μm. Detector apertures from 50 μm to 3 mm are available which allows us to choose the ratio of detector area to coherence area over a wide range. A typical setting of 400 μm would give a ratio between 1/4 and 4, which implies that less than four coherence areas strike the detector. Observations of scattering from dilute suspensions of standard latex particles show that with the optics as described, the amplitude of the field autocorrelation function approaches the ideal limit of one as the aperture diameter is decreased to one coherence area and further toward the limit of a point detector. This is in agreement with the results of Jakeman and many others for a well designed dynamic light scattering instrument[15].

With the goniometer and correlator as described we have no problem meeting the recommendations of Oliver[15] for optimal determination of correlation decay constants. We observe a random error in the measured decay constant which is quite small. With carefully prepared samples $\Delta\Gamma/\Gamma$ is always less than $\pm 0.5\%$. This precision of measurement is over an order of magnitude better than observed in Oliver's simulations. The increased precision is primarily due to the fact that our experiments typically accumulate $>10^7$ samples compared to $\leqslant 10^5$ in Oliver's simulations.

Some compromises are necessary in using this goniometer for measuring total intensity scattering. We note however that with current instrumentation the compromises are no longer as severe as was once the case (and is often still supposed). The most common problems are lack of reproducible scattering volume size, instability of laser source intensity or pointing, and the necessity of significant corrections due to refractive indices of solvents. Use of a focused incident beam accentuates each of these potential problems. Fundamentally, they would all be manifested as systematic deviations of the volume

corrected scattering intensity vs. angle. For our static light scattering analysis we have applied a geometric volume correction, multiplying intensity by $(\sin\theta)$ as discussed above, and we have corrected for fluctuations in incident laser intensity by monitoring the straight through beam with a separate PMT. These simple corrections alone provide data which is free from systematic deviations to within $\pm 0.5\%$ for scattering angles from 30 to 150°. Furthermore, as will be observed in the Zimm plots presented below, because any remaining systematic errors occur in scattering from blank as well as sample solutions, their effects are even further reduced.

We can speculate on the reasons why the data quality is better than might be expected from a compromised design. First, the goniometer itself is of very high quality with precision machining and adjustments for optimal alignment which can be rigorously checked. The laser and optics are also securely mounted on a stable optical table. Second, in the detection optics the final scattering volume image is defined by a vertical slit so that we minimize the effects of slight variations in detector height as a function of angle. We expect that this would be the most likely mechanical problem. The influence on the measured intensity is further reduced by placement of a diffusion plate after the slit and before the photocathode of the PMT. A photocathode usually has non-uniform sensitivity across its surface and the diffusion plate reduces effects of beam wander by providing more uniform illumination of the photocathode surface.

Other errors in the absolute intensity can arise from differences in refractive indices for the index matching vat liquid, calibration liquid, and polymer solution. The measured solid angle is proportional to $(n_s/n_c)^2$ where n_s and n_c are the refractive indices of the solution and calibration liquid, respectively. In the measurements reported here toluene was used for each of these liquids so refraction corrections are not necessary. A calibration for the Rayleigh ratio of toluene was referenced to benzene but the refraction correction in that case is less than 0.5%, which is smaller than the uncertainty associated with the Rayleigh ratio of benzene itself.

It should be noted that the focused beam optical design used in this goniometer also provides some advantages over a traditional large beam static instrument. For our concentric glass cells the focused beam enters and leaves normal to the scattering cell, thus minimizing stray reflections. The most significant advantage of the focused beam is that spurious scattering from remaining dust particles will be observed by our automated data acquisition and dust discrimination software as enormous deviations in scattering intensity as particles float through the small region of high power density. Instead of averaging over a large volume which may at any time contain one or more anomalous scatterers, we easily detect and automatically reject deviant occurrences on a real time basis. Indeed, the knowledge that large fluctuations occur in the static scattering provides a diagnostic tool which alerts us to potential anomalies in the dynamic scattering correlation functions.

Electronics. The photon correlation measurements were performed with a 264 channel multibit autocorrelator (Brookhaven Instruments 2030). A separate 20 MHz photon counter was used in parallel with the correlator to measure the total scattered and transmitted intensities. An optional phase locked beam chopper was used to correct for PMT dark counts but they were found to be so low (<5 cps) that they were neglected in most experiments. The correlator, counter, and goniometer stepping motor were all controlled by a dedicated microcomputer (IBM PC type) for automatic data acquisition. The correlation data was then transferred to a VAX 11/780 computer where it could be analysed with non-linear least squares fitting programs.

As will be shown later, the counting efficiencies of the correlator and the photon counter are matched to within 0.01%, independent of count rate up to 2.5×10^5 cps. The photon counter serves three purposes in our experiment. First, it is used to check for spurious scattering from dust or other sample impurities. Non-statistical fluctuations in the values of the intensity are determined by taking 10^2 to 10^4 individual samples and sorting them into a histogram of values from which the outliers (taken to be those more than ± 2 standard deviations from the mean) are rejected. For data from well prepared samples, the average intensities before and after this procedure are usually within 0.02%. At low angles, where large particle scattering is highest, the discrimination procedure can improve the results. To apply the same scheme to d.l.s. would require acquisition of a large number of correlation functions which could, with post-processing, be combined. We have not attempted this.

The second purpose of the photon counter is to provide a background calibration to account for drift in laser intensity. In practice, we find the intensity and pointing stability of our laser to be excellent, such that the correction for drift is minor. The third use of the counter is to provide a clear comparison to determine the calibration of the calculated correlation function baseline values, which will be used in this set of experiments to produce integrated total intensity Zimm plots.

Sample preparation

The polymer samples used for this study were commercially available standards of anionically polymerized polystyrenes ranging in molecular weight from 1.79×10^5 to 20×10^6. They are described in *Table 1*. The concentrations used are all below the overlap concentration, c^*. As with all light scattering experiments, cleanliness of polymer solutions and scattering cells is essential. All solutions were prepared using toluene which had been dried over liquid sodium, distilled and filtered several times with 3.0, 1.0, and 0.2 μm membrane filters (Millipore). Stock solutions were prepared by weight and allowed to equilibrate at 35°C for several days or weeks with occasional gentle agitation. Scattering cells were prepared from selected 12 mm borosilicate reaction tubes which were thoroughly cleaned. Directly before use the prepared cells were rinsed with distilled toluene vapours and inspected again for scratches and dust. The dilute stock solutions

Table 1 Description of polymer samples

Sample	$M_w \times 10^{-6}$ (g mol^{-1})	M_w/M_n	c^* (calc.) (mg ml^{-1})	Concentration range (mg ml^{-1})
NBS 705	0.179	1.05	11.2	0.50–5.0
NBS 1479	0.05	1.1	3.01	0.20–2.0
Toyo Soda 550	5.50	1.2	1.11	0.05–0.50
Toyo Soda 2000	20.0	<1.3	0.451	0.03–0.15

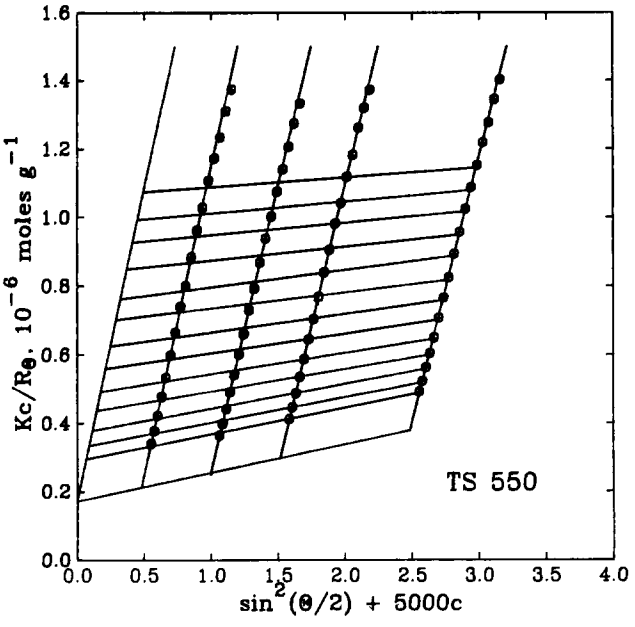

Figure 2 Static light scattering analysis of 5.5×10^6 molecular weight polystyrene in toluene with dust discrimination software, ○, and raw data without dust discrimination, +

were filtered into the scattering cells where they were diluted to the desired concentrations by weight with additional filtered toluene. Cells were flame sealed under vacuum and allowed to equilibrate at 35°C for 1 to 6 weeks. The samples included in these measurements showed no speckles, spurious scattering, or irregularities in the scattering functions.

RESULTS AND DISCUSSION

The excess absolute intensity of scattered light from a dilute polymer solution with concentration c and at an angle θ has the form[3]

$$Kc/R_v(\theta) = (1/M_w)(1/P(\theta) + 2A_2c \quad (1)$$

where the optical constant

$$K = (4\pi^2 n^2/N_a\lambda_0^4)(\partial n/\partial c)_t^2$$

and the static structure factor

$$P(\theta) = [1 + (q^2\langle R_G^2\rangle_z/3) + \text{higher order terms}]^{-1}$$

with n, λ_0, $(\partial n/\partial c)_t$, M_w, $\langle R_G^2\rangle_z$, q $[\equiv (4\pi n/\lambda_0)\sin(\theta/2)]$, and A_2 being respectively, the index of refraction of solvent, the wavelength of light in vacuum, the refractive index increment of the system at constant temperature, the weight average molecular weight, the z-average radius of gyration, the magnitude of the momentum transfer vector, and the second virial coefficient. The v subscript indicates that the incident light has a vertical polarization while the detector collects light of all polarizations. $Kc/R_v(\theta)$ is calculated from known constants: $n_{tol} = 1.4961$; $(\partial n/\partial c)_{tol} = 0.110$; $R_{vv}(\theta) = 24.2 \times 10^{-4}$ (as recently reported by Moreels *et al.*[16]) for $\lambda = 514.5$ nm and 25°C. The corresponding value of $R_v(\theta)$ is calculated[17] as $R_v = R_{vv}(1 + \rho_v)$ where ρ_v is the depolarization ratio for the solvent taken from Pike *et al.*[18] as $\rho_v = 0.31$. Our instrument is thus calibrated by the ratio $R_{cal}^{90^\circ} = R_v/I_{solvent}^{90^\circ}$. Using this calibration constant, the measured scattering intensities for solution and solvent are converted to $Kc/R_v(\theta)$ values in units of $1/M_w$ with the relationship

$$Kc/R_v(\theta) = [1/(I_{solution}(\theta) - I_{solvent}(\theta))][Kc/R_{cal}^{90^\circ}] \quad (2)$$

As is customary, these Kc/R_θ values are plotted against $\sin^2(\theta/2) + kc$ where k is an arbitrary constant. Data at constant θ or c are fit with least squares and extrapolated to $c = 0$ and $\theta = 0$. The double extrapolation yields M_w as the joint intercept, while R_G and A_2 are determined from the ratio slope/intercept of the $c = 0$ and $\theta = 0$ lines, respectively. *Figure 2* shows the s.l.s. analysis of TS550 in toluene. The data shown with circles and crosses are with and without dust discrimination, respectively. We note, as was stated earlier, that for these carefully prepared samples the discrimination procedure has no significant influence on the results.

The photocount (intensity) autocorrelation function $G^{(2)}(\tau)$ is related to the scattered field autocorrelation function $g^{(1)}(\tau)$ by the Siegert relationship[13]

$$G^{(2)}(\tau) = A(1 + \beta|g^{(1)}(\tau)|^2) \quad (3)$$

where A is the average uncorrelated scattering intensity and β is an instrument parameter which is $\leqslant 1$. Experimentally $G^{(2)}(\tau)$ is measured by the digital autocorrelator as the summation

$$G^{(2)}(k\Delta\tau) = \lim_{N\to\infty} \frac{1}{N} \sum_{i=1}^{N} n_i n_{i+k} \qquad k = 1, 2, 3, \ldots, 264 \quad (4)$$

where n_i counts are collected during each interval $\Delta\tau$. In practice the $1/N$ factor is included in the background constant A of equation (3) and therefore the absolute magnitude of $G^{(2)}$ depends on experiment duration. The absolute magnitude of $G^{(2)}(\infty)$, the infinite time 'far point' value, is equal to $\langle I\rangle^2$, the square of the average total scattering intensity. We therefore remove the dependence of $G^{(2)}(\tau)$ and $G^{(2)}(\infty)$ on the experimental parameters of experiment duration and sampling interval to extract values equivalent to the s.l.s. data as

$$I(\theta) = \sqrt{A(\theta)/N\Delta\tau^2} \quad (5)$$

where $A(\theta)$ could be the counts in long time delay channels or it could be the calculated far point given by

$$A(\theta) = \frac{(\text{total counts} - \text{overflows})(\text{prescaled counts})}{(\text{number of samples})} \quad (6)$$

We have used the calculated $A(\theta)$ although it would not matter here because the calculated and measured baselines were the same to within 0.02%.

For these experiments, overflows were negligible (<50) and no input prescaling was used. With the long τ values of the d.l.s. autocorrelation function, reduced as in equation (5), we constructed Zimm plots such as are shown with crosses in *Figure 3*. The circles are from concurrent s.l.s. data as were shown in *Figure 2*. The agreement is excellent between the two sets of data.

There are three possible instrumental reasons for any differences which may occur between data analysed in this manner. First, inherent differences in the counting efficiencies of the electronics; second, overflows of the 4 bit input counter on the correlator; third, the use of the dust discrimination routine in the collection of the static data only.

The effect of overflows is kept very small as is demonstrated in *Figure 4*, which is a plot of counts per second taken from s.l.s. *versus* those from d.l.s. by this treatment. The experiment duration varies from 1 to 15 minutes, the

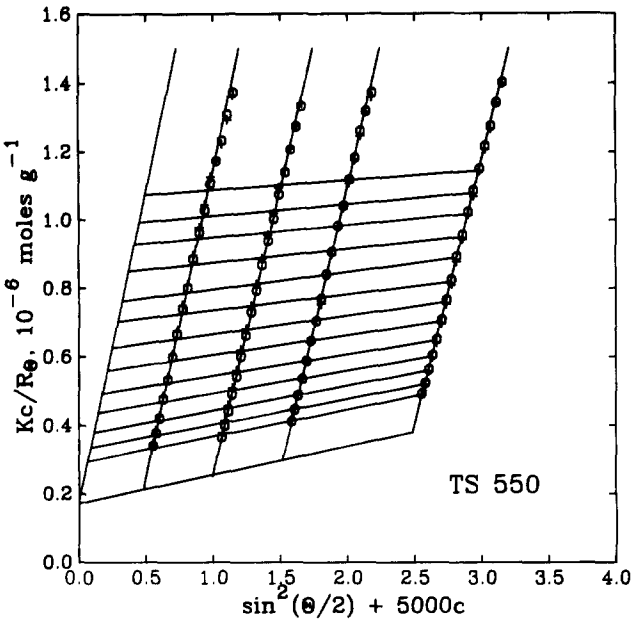

Figure 3 Static light scattering analysis of TS550 polystyrene in toluene. ○, Same as *Figure 2*; +, determined by analysis of concurrent dynamic light scattering correlation functions

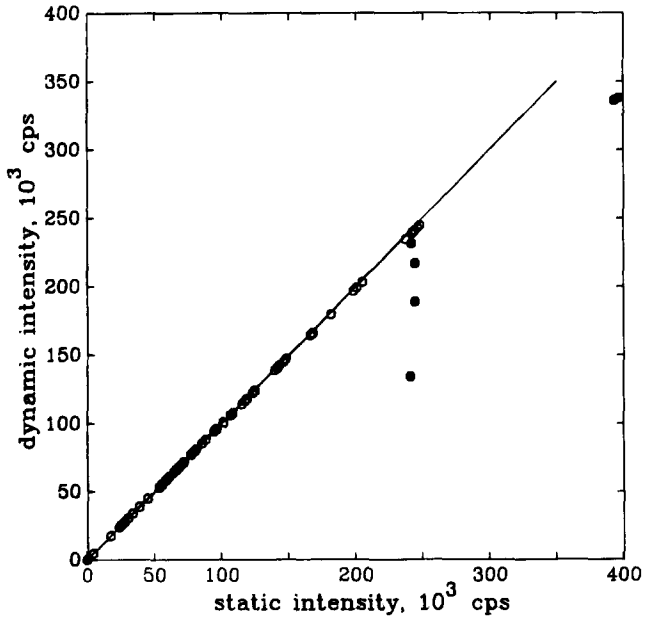

Figure 4 Comparison of total intensity counts determined from d.l.s. against the simultaneous s.l.s. detection. The line is drawn with a slope of 1.00. Deviations are the result of excessive overflows (>5% of total counts) from autocorrelator input shift registers

correlator sample time from 1 μs to 1 ms. When there are no overflows, which is usually the case, d.l.s. and s.l.s. intensity numbers are very close. In this figure, filled points represent data taken with overflows intentionally allowed to exceed 5% and they clearly deviate. The electronic efficiencies of the two 'counters' are the same to within 0.5%.

The usual purpose of a d.l.s. experiment is determination of diffusion coefficients. For isolated, noninteracting monodisperse scattering molecules $g^{(1)}(\tau)$, the normalized correlation function is given by[13]

$$g^{(1)}(\tau) = \mathscr{A} e^{-\Gamma\tau} \quad (7)$$

where $\Gamma = Dq^2$, with D the mutual diffusion coefficient. Polydisperse samples and systems with contributions from internal chain fluctuations are often modelled with a cumulant expansion of decay constants which reflect the breadth in the distribution of relaxation processes. *Figure 5* shows Γ vs. q^2 for the NBS 705 sample at 4 concentrations and is typical of our d.l.s. data for moderate molecular weight samples. *Table 2* gives the results of the complete concurrent static and dynamic analysis of all the samples listed in *Table 1*. The analyses are extremely consistent across the entire set of s.l.s. and d.l.s. measurements. The relationship between R_G and R_H is consistent with that reported by others[20].

The Zimm plots for TS2000, a 20×10^6 molecular weight polymer, show significant curvature beginning around 60° as intraparticle scattering influences $P(\theta)$. In order to extract meaningful parameters from a Zimm plot with curvature such as this, higher order terms must be included in the expression for $P(\theta)$ as given in equation (1). Alternatively, we can restrict our Zimm analysis to lower angle values and approach the limiting slopes of the constant concentration data sets to deduce M_w, R_G, and A_2 as shown in *Figure 6*. Another approach would be to fit the data with an analytical expression for $P(\theta)$ using a particular model. Fundamentally, we are observing the onset of contributions to the static scattering from intraparticle interferences.

From the perspective of dynamic scattering, the crossover region where internal chain fluctuations contribute to the correlation functions, is observed in the substantial deviation from the usual $\Gamma = Dq^2$ dependence of decay constant on wave vector. *Figure 7* combines data for three molecular weights plotted as Γ/q^2D_0 vs. qR_G where D_0 is the infinite dilution diffusion coefficient which serves to normalize the different molecular weights. The d.l.s. clearly shows the crossover into the expected q^3 dependence occurring at qR_G near 1. By observing this d.l.s. crossover we remark that the TS550 scattering is strongly in the q^3 internal mode region. At the same time *Figures 2* and *3* show that s.l.s. (even when deduced from d.l.s. correlation functions) does not seem to deviate on the Zimm plot analysis. The appearance of deviations from

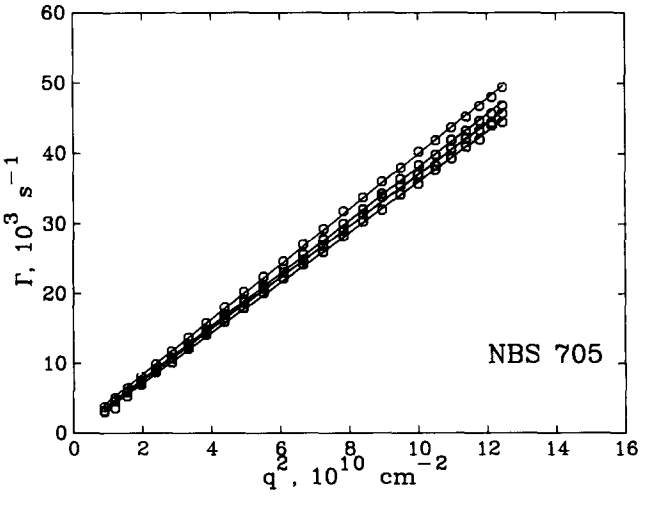

Figure 5 Dynamic light scattering decay constant Γ against q^2 for several concentrations (1.2–5.0 mg ml^{-1}) of 1.79×10^5 molecular weight polystyrene. The diffusion coefficient, given by slope, decreases with decreasing concentration as has been observed by others[19]

Table 2 Results of complete concurrent static and dynamic analysis of samples

Sample	Static light scattering			Dynamic light scattering				
	$M_w \times 10^{-6}$ (g mol^{-1})	R_G (nm)	$A_2 \times 10^4$ (cm^3 mol g^{-2})	$M_w \times 10^{-6}$ (g mol^{-1})	R_G (nm)	$A_2 \times 10^4$ (cm^3 mol g^{-2})	$D_0 \times 10^7$ (cm^2 s^{-1})	R_H (nm)
NBS 705	0.191	18.2	6.00	0.198	19.7	5.87	3.49	11.1
NBS 1479	0.939	47.4	4.00	0.957	49.3	4.18	1.44	26.8
Toyo Soda 550	5.85	154	2.09	5.42	149	1.93	0.62	62.2
Toyo Soda 2000	15.9	282	1.61	16.2	285	1.60	(0.31) (estimated)	(124)

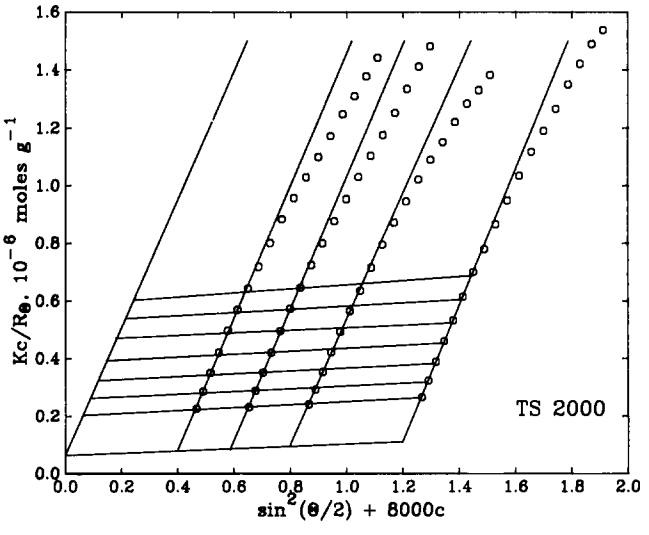

Figure 6 S.l.s. analysis of 20×10^6 molecular weight polystyrene in toluene. Contribution of high order terms to the particle scattering factor causes deviations at angles above 60° corresponding to $qR_G = 5$

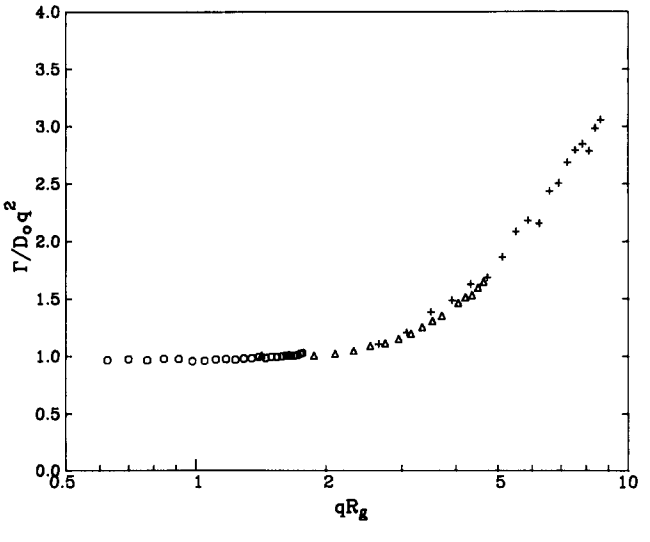

Figure 7 D.l.s. delay constant, reduced by q^2 and the infinite dilution diffusion coefficient, D_0, plotted against $\log qR_G$ for: ○, NBS1479; △, TS550 and +, TS2000. The transition to q^3 dependence occurs at $qR_G \approx 2$

the straight lines of the Zimm plot do occur but they are at about an order of magnitude higher value of qR_G (cf. *Figure 6*).

Some difference of this type is expected. Akcasu *et al.*[6] have discussed in detail how the dynamic structure factor $S(q, \tau)$ reflects the crossover behaviour. Their analysis specifically treats the $\tau \to 0$ limiting value of the first

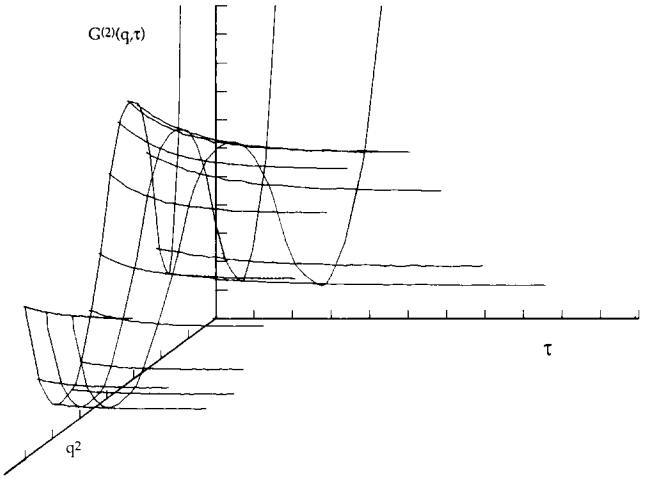

Figure 8 D.l.s. function $G^{(2)}(q, \tau)$ for dilute latex suspensions, reduced to absolute scattering intensity functions, are plotted against τ and q^2. Correlation functions are connected at several constant $q^2\tau$ values. The shape of the contours follows a solid sphere scattering function

cumulant of $S(q, \tau)$ to determine a characteristic relaxation time. They also show that the relative contributions of different relaxation modes to $S(q, \tau)$ depends on τ as well as q.

Another case where $P(\theta)$ becomes very interesting is for large particles such as lattices in suspension. Here $P(\theta)$ can be calculated from a particular model function such as that for solid spheres[11]

$$P(\theta) = [(3/u^3)(\sin u - u \cos u)]^2 \quad (8)$$

with $u = qr$ and r the sphere radius. This function can be applied to integrated scattering intensity data derived from either s.l.s. and d.l.s. Instead, in *Figure 8* we have reduced a set of measured $G^{(2)}(q, \tau)$ functions by the experimental parameters, in the same manner as equation (5) was used on the far point value. The resulting scattering surface is drawn as correlated intensities vs. q^2 on one axis and τ on the other. Because there are no internal modes or extraneous sources of scattering the static data (in q space) can be described by equation (8) and the dynamic (in τ space) by equation (7). We may expect some difference between the hydrodynamic radius (which is reflected in the diffusion coefficient) and the sphere radius (for equation (8)). For solid spheres the difference is seen to be quite small from an independent fitting of s.l.s. and d.l.s. For this figure we have connected contours between the correlation function decays along values of constant $q^2\tau$ values consistent with equation (7).

CONCLUSIONS

We have demonstrated that the d.l.s. autocorrelation function can be put on an absolute scale. This leads to a complete analysis of the static and dynamic molecular properties of molecular weight, radius of gyration, virial coefficient and diffusion coefficient. Both of our test systems, dilute polymer solutions and dilute latex suspensions, are simple systems for which there is a fundamental relaxation process corresponding to the properties of the whole molecule. It would have been very surprising if we had failed to obtain consistent results for these model systems and indeed the results are of excellent quality. While the method we have described here may have some utility for analysis of well defined scattering systems, the real application will be to systems with complex scattering processes. Even in this work we have suggested that the q^2 to q^3 crossover region where internal relaxations are observed may benefit from a consistent s.l.s./d.l.s. analysis. Subsequent work in the application of this method will be to multimodal scattering systems such as semidilute solutions, polyelectrolyte and stiff chain solutions, and ternary polymer–polymer–solvent systems.

ACKNOWLEDGEMENTS

The work was supported in part by the donors of the Petroleum Research Fund, administered by the American Chemical Society. We have also benefited from discussions with Dr Bruce Weiner of Brookhaven Instruments.

REFERENCES

1 Amis, E. J. and Han, C. C. *Polymer* 1982, **23**, 1403
2 Amis, E. J., Han, C. C. and Matsushita, Y. *Polymer* 1984, **25**, 650
3 Brown, W. *Macromolecules* 1984, **17**, 66
4 Adam, M. and Delsanti, M. *Macromolecules* 1985, **18**, 1760
5 Eisele, M. and Burchard, W. *Macromolecules* 1984, **17**, 1636
6 Akcasu, A. Z., Benmouna, M. and Han, C. C. *Polymer* 1980, **21**, 866
7 Stock, R. S. and Ray, W. H. *J. Polym. Sci., Polym. Phys. Edn.* 1985, **23**, 1393
8 Martin, J. E. *Macromolecules* 1986, **19**, 922
9 Borsali, R., Duval, M., Benoit, H. and Benmouna, M. *Macromolecules* 1987, **20**, 1112
10 Wheeler, L. M., Lodge, T. P., Hanley, B. and Tirrell, M. *Macromolecules* 1987, **20**, 1120
11 Phillies, G. D. J. and Billmeyer, F. W. in 'Treatise in Analytical Chemistry' (Eds P. J. Elving and E. J. Meeham), Wiley, New York, 1986, Part 1, Section H, Ch. 9
12 Chen, S.-H., Chu, B. and Nossal, R. Eds, 'Scattering Techniques Applied to Supramolecular and Nonequilibrium Systems', Plenum Press, New York, (1980)
13 Pecora, R. 'Dynamic Light Scattering', Plenum Press, New York (1985)
14 Chu, B. 'Laser Light Scattering', Academic Press, New York (1974)
15 Oliver, C. J. *Advances in Physics* 1978, **27**, 387
16 Moreels, E., De Ceuninck, W. and Finsy, R. *J. Chem. Phys.* 1987, **786**, 618
17 Utiyama, H. in 'Light Scattering from Polymer Solutions' (Ed. M. B. Huglin), Academic Press, London, 1972, Ch. 4
18 Pike, E. R., Pomeroy, W. R. M. and Vaughan, J. M. *J. Chem. Phys.* 1975, **632**, 3188
19 Adam, M. and Delsanti, M. *Macromolecules* 1977 **10**, 1229
20 Adam, M. and Delsanti, M. *J. de Physique* 1976, **37**, 1045